HPSTAR
067_2014

PHYSICAL REVIEW B **90**, 094115 (2014)

Bond deformation paths and electronic instabilities of ultraincompressible transition metal diborides: Case study of OsB_2 and IrB_2

R. F. Zhang,[1,2,3] D. Legut,[4] X. D. Wen,[2,5] S. Veprek,[6] K. Rajan,[3] T. Lookman,[2] H. K. Mao,[7,8] and Y. S. Zhao[9]

[1]*School of Materials Science and Engineering, and International Research Institute for Multidisciplinary Science, Beihang University, Beijing 100191, P. R. China*

[2]*Theoretical division, Los Alamos National Laboratory, Los Alamos, New Mexico 87545, USA*

[3]*Department of Materials Science and Engineering, Iowa State University, Ames, IA50010, USA*

[4]*Nanotechnology Centre, VSB-Technical University of Ostrava, CZ-708 33 Ostrava, Czech Republic*

[5]*State Key Laboratory of Coal Conversion, Institute of Coal Chemistry, Chinese Academy of Sciences, P.O. Box 165, Taiyuan, Shanxi 030001, P. R. China & Synfuels China, Beijing 100195, P. R. China*

[6]*Department of Chemistry, Technical University Munich, Lichtenbergstr. 4, D-85747 Garching, Germany*

[7]*Geophysical Laboratory, Carnegie Institution of Washington, NW Washington, DC 20015, USA*

[8]*Center for High Pressure Science and Technology Advanced Research, Shanghai 201203, P. R. China*

[9]*HiPSEC, Department of Physics and Astronomy, University of Nevada, Las Vegas, NV 89154, USA*

(Received 9 March 2014; revised manuscript received 29 August 2014; published 26 September 2014)

The energetically most stable orthorhombic structure of OsB_2 and IrB_2 is dynamically stable for OsB_2 but unstable for IrB_2. Both diborides have substantially lower shear strength in their easy slip systems than their metal counterparts. This is attributed to an easy sliding facilitated by out-of-plane weakening of metallic Os-Os bonds in OsB_2 and by an in-plane bond splitting instability in IrB_2. A much higher shear resistance of Os-B and B-B bonds than Os-Os ones is found, suggesting that the strengthened Os-B and B-B bonds are responsible for hardness enhancement in OsB_2. In contrast, an in-plane electronic instability in IrB_2 limits its strength. The electronic structure of deformed diborides suggests that the electronic instabilities of 5*d* orbitals are their origin of different bond deformation paths. Neither IrB_2 nor OsB_2 can be intrinsically superhard.

DOI: 10.1103/PhysRevB.90.094115 PACS number(s): 62.20.de, 61.50.Ah, 62.20.M−, 71.20.Ps

The ultraincompressibility ($B > 250$ GPa) and possible superhardness ($H_v \geq 40$ GPa) of transition metal (*Tm*) borides has stimulated tremendous interest in theoretical and experimental investigations of their properties [1–5]. The ultraincompressibility of borides of 5*d* transition metals, such as OsB_2 [4], ReB_2 [5], WB_2 [6], IrB_2 [7], and WB_3 [8] and others, is widely accepted, but the experimentally determined load-invariant hardnesses are typically below 30 GPa, i.e., these materials are not superhard. Osmium diboride possesses high elastic moduli but a low hardness due to the presence of Os-Os weak metallic bonds [9]. Rhenium diboride was believed to be superhard [5], but its load-invariant hardness is also less than 30 GPa because of electronic instabilities of 5*d* orbitals under finite shear strain resulting in transformation to phases with lower plastic resistance [10]. Tungsten diboride was originally proposed as another superhard material with "predicted" hardness of 46 GPa [6], but the experiment yields only 30 GPa [11]. Iridium borides received much attention because of the Vickers hardness of 49.8–18.2 GPa reported for $IrB_{1.35}$ at loads of 0.49 and 9.81 N, respectively [12]. However, as discussed in [13], only the low value of 18.2 GPa measured at high load is the correctly measured load-invariant hardness. The energetically favored orthorhombic structure of IrB_2 is isostructural to OsB_2 [7], in which Os-Os metal double layers in the easiest slip system limit its anisotropic shear strength to about 9 GPa [7,9].

The presence of metal double layers in diborides of 5*d* transition metals is believed to be the origin of their low hardness. However, studies of bond deformation paths and electronic instabilities under shear deformation, which have been shown to be critical in several ultraincompressible materials [10,14], are lacking. In many papers the conclusions are mostly based on the development of atomic structure and bond topology under shear, but the related electronic instabilities of 5*d* orbitals remain unexplored. Taking OsB_2 and IrB_2 as examples, we show for the first time that, although easily sliding metal double layers exist in both diborides, their shear deformation paths are substantially different. In addition, in spite of a significant weakening between the Os-Os layers in OsB_2, the hardness of OsB_2 of almost 30 GPa is significantly higher than the shear strength of the easy slip system, because, under the conditions of plastic flow, all slip systems must shear to meet the compatibility condition (constant volume). Thus it is interesting to investigate the origin of the weakening of Os-Os layers and the shear resistance of the Os-B and B-B layers.

The 30 GPa hardness of OsB_2 can be understood in terms of complex deformation beneath the indenter upon the measurement, as described by slip-line fields [15,16]. Accordingly, the material upon indentation displays a complex flow where many slip systems, including the strong ones, are activated. Moreover, correctly measured, load-invariant hardness describes the mechanical behavior of strongly deformed material with a large density of flaws. Therefore the recent "theories of hardness" [17–19] describe only the elastic stiffness of an ideal crystal but not real hardness [20].

Our calculations of phonon dispersion of OsB_2 and IrB_2 show that whereas OsB_2 is dynamically stable in its lowest energy structure, IrB_2 is unstable. This result contradicts the previous results by Wang *et al.* [21], who suggested that IrB_2 is dynamically stable. Furthermore, we show that although both OsB_2 and IrB_2 have the same equilibrium structure, their bond deformation paths are substantially different due to different electronic instabilities under shear.

 ©2014 American Physical Society

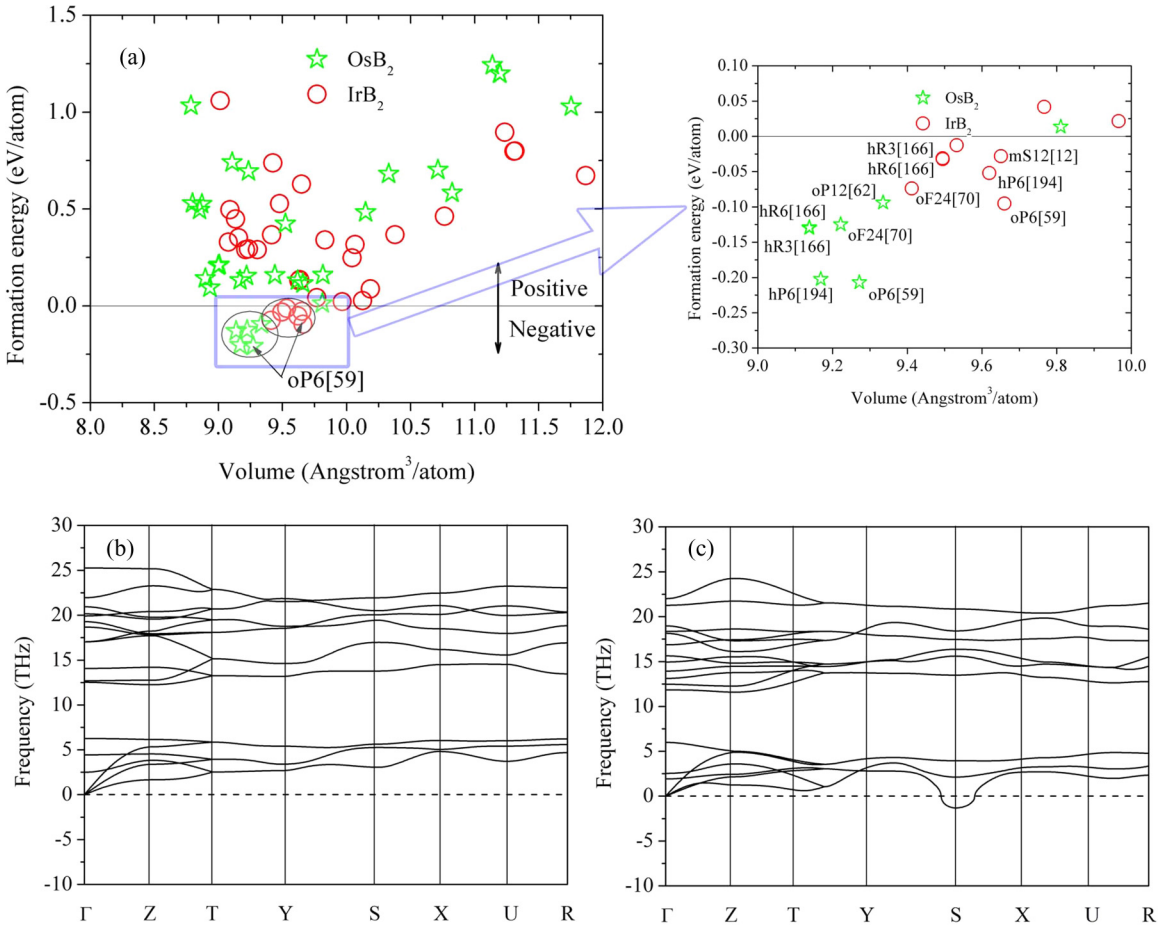

FIG. 1. (Color online) (a) Formation energy of OsB_2 and IrB_2 calculated by DFT to determine the possible ground-state phases of 33 commonly observed *Tm*-B, *Tm*-C, *Tm*-N, *Tm*-Al, *Tm*-Si ICSD structure types and the newly reported diborides by the crystal structure evolutionary search method. Calculated phonon dispersion curves for (b) OsB_2 and (c) IrB_2 in *oP*6[59] structure.

We first show that *oP*6[59] structure (expressed by Pearson symbol and space group number in bracket) of IrB_2 and OsB_2 is energetically favorable. We use the VASP code [22] to perform first-principles density functional theory (DFT) calculations of the formation energy of OsB_2 and IrB_2 in more than 30 commonly observed *Tm*-B, *Tm*-C, *Tm*-N, *Tm*-Al, and *Tm*-Si ICSD structure types [23] and in the diboride structures by means of the "high-throughput" evolutionary search method [21,24,25]. (See the Supplemental Materials [26] for details of the OsB_2 and IrB_2 structures.) All studied structures were relaxed with respect to both lattice parameters and atomic positions. Based on the reaction $Tm + 2\mathrm{B} = TmB_2$, the formation energy was calculated as $\Delta E = \frac{1}{3}[E(TmB_2) - E(Tm) - 2E(\mathrm{B})]$, with $\alpha - \mathrm{B}$ and *Tm* in their ground states. Figure 1(a) summarizes the calculated formation energies vs volume at 0 K. The stable and metastable structures with formation energy close to zero are shown in the inset of Fig. 1(a). Obviously, *oP*6[59] has the lowest formation energy for both OsB_2 and IrB_2.

We next study the dynamical properties of both OsB_2 and IrB_2 in five selected structures reported in [23], using the direct method [27] as employed by the PHONOPY code [28]. The boron layers in these structures are flat in *hP*3[191], armchair in *oP*6[59], zigzag in *hP*6[194], alternately flat and zigzag in *hP*12[194], and nonequal zigzag in *hR*6[166]. The resulting phonon dispersion and density of states (PDOS) were the same as those using the $2 \times 2 \times 2$ supercell method. Figures 1(b) and 1(c) show the dispersion relations of OsB_2 and IrB_2 in *oP*6[59], indicating a dynamic stability for OsB_2, as there are no modes with imaginary frequencies, but dynamic instability of IrB_2, as there are imaginary frequencies at the high-symmetry *S* point [0.5 0.5 0.0]. The partial PDOS of IrB_2 and OsB_2 indicate that the lower frequencies of the total PDOS are dominated by lattice dynamics of heavy Ir (Os) atoms and higher frequencies by light B atoms. Imaginary frequencies found for IrB_2 with *oP*6[59] structure are given exclusively by the atomic vibrations of Ir atoms. There is a gap in phonon frequencies between ca. 6.8 (7.2) and 10.9 (11.6) THz in IrB_2 (OsB_2) that entirely separates higher and lower frequencies. For the high-energy structures we found that OsB_2 is dynamically unstable in several important directions in *hP*3[191], *hP*12[194], and *hR*6[166] but is stable in the *hP*6[194] structure. In contrast, the IrB_2 is dynamically instable in all these structures.

To evaluate the elastic stability [29] of both diborides, we calculated their single-crystal elastic constants using both a linear response method and efficient strain-energy method [30]. The obtained elastic constants of IrB_2 (C_{11}= 349 GPa, $C_{22} = 414$ GPa, $C_{33} = 668$ GPa, $C_{44} = 68$ GPa, $C_{55} =$ 62 GPa, $C_{66} = 132$ GPa, $C_{12} = 244$ GPa, $C_{13} = 145$ GPa, and $C_{23} = 167$ GPa) and of OsB_2 ($C_{11} = 565$ GPa, $C_{22} = 538$ GPa,

TABLE I. Voigt average bulk modulus B_V, shear modulus G_V (both in GPa), and the ideal strength (minimum tensile strength σ_{min} and shear strength τ_{min}) of OsB_2, IrB_2, metal Os, and Ir calculated by first-principles methods. Previous theoretical results for Re_3N [14], ReB_2 [30], WB_3 [33], B_6O [34], c-BN [35], and diamond [34,36] are included for comparison.

Compound	Reference	a	b	c	B_V	G_V	σ_{min}	τ_{min}
OsB_2	This study	2.89	4.71	4.10	313	181	37.6	9.2 (36.6*)
	[7]	2.89	4.71	4.10	312	158		
Os	This study	2.76	2.76	4.35	400	254	35.6	22.2
	[31]				410	274		
IrB_2	This study	3.16	4.55	4.05	280	110	23.7	7.9 (15.7*)
	[21]	3.15	4.55	4.04	277	108		
Ir	This study	3.88	3.88	3.88	345	218	27.1	18.6
	[32]				355	221		
Re_3N	[14]	2.83		7.19	397	203	34.5	15.5
ReB_2	[30]	2.92		7.52	348	274	58.5	34.4
WB_3	[33]	5.20		6.34	293	245	43.3	37.7
B_6O	[34]	5.39		12.3	231	218	53.3	38.0
c-BN	[35]				376	390	55.3	58.3
Diamond	[34,36]				442	528	82.3	86.8

*The shear strengths are calculated by a confined deformation scheme to restrict the Me-Me bilayer sliding.

$C_{33} = 763$ GPa, $C_{44} = 191$ GPa, $C_{55} = 73$ GPa, $C_{66} = 193$ GPa, $C_{12} = 178$ GPa, $C_{13} = 185$ GPa, and $C_{23} = 130$ GPa) are in good agreement with the previous calculations (for IrB_2, $C_{11} = 353$ GPa, $C_{22} = 416$ GPa, $C_{33} = 676$ GPa, $C_{44} = 69$ GPa, $C_{55} = 68$ GPa, $C_{66} = 140$ GPa, $C_{12} = 239$ GPa, $C_{13} = 138$ GPa, and $C_{23} = 171$ GPa [21], for OsB_2, $C_{11} = 547$ GPa, $C_{22} = 537$ GPa, $C_{33} = 748$ GPa, $C_{44} = 189$ GPa, $C_{55} = 62$ GPa, $C_{66} = 193$ GPa, $C_{12} = 178$ GPa, $C_{13} = 192$ GPa, and $C_{23} = 130$ GPa [7]). The calculated independent elastic constants for both phases satisfy the lattice stability criteria [29]. The Voigt bulk modulus B_V and shear modulus G_V are listed in Table I in comparison with other transition metal borides, and superhard B_6O, BN, and diamond [7,14,21,30–36]. The high values of bulk moduli of IrB_2 and OsB_2 suggest they are ultraincompressible; however, their shear moduli are even lower than those of their metal counterparts, indicating a low shear stiffness.

Whether a crystalline solid is ductile or brittle can be characterized by the so-called Pugh ratio of the averaged shear modulus to the bulk modulus, G/B [37]. The critical G/B ratio which separates ductile and brittle materials is around 0.57, i.e., if $G/B < 0.57$ the material behaves in a ductile manner, otherwise it is brittle [37]. The low ratio of $G/B \approx 0.39$ for IrB_2 suggest that it is ductile, while OsB_2 with $G/B \approx 0.58$ should be brittle.

In order to obtain a deeper understanding of the difference between IrB_2 and OsB_2 in their response to strain, the valence charge density differences (VCDDs) are calculated and compared in Fig. 2. The differences between the two diborides are as follows: the in-plane Ir-Ir bond distances of 3.16 Å in IrB_2 are longer than the out-of-plane distances at 3.07 Å, whereas in OsB_2 the in-plane Os-Os bond lengths of 2.89 Å are shorter than the out-of-plane lengths at 3.04 Å. Such difference is due to the significant accumulation of valence charge density within boron layers in OsB_2, as seen in Figs. 2(a) and 2(b). To elucidate the origin of this difference, the calculated partial electronic density of states (EDOS) are shown in Figs. 2(c) and 2(d). Both diborides show metallic bonding because of finite value of EDOS at the Fermi level (E_F), which originate mostly from d electrons of Ir and Os and the p electrons of B. In OsB_2, the EDOS at E_F shows a pseudogap, i.e., a stronger localization of valence electrons. In IrB_2, however, the flat nature of EDOS around E_F indicates a delocalization. The strengthened B-B bonds in OsB_2 cause a denser in-plane packing of Os-Os layers, while the delocalized B-B bonds make in-plane Ir-Ir bonds even longer. The Bader charge density analysis [38] shown in Figs. 2(a) and 2(b) further confirms the positive (negative) charge transfer from Os (Ir) atoms to boron atoms, supporting further the strengthening (weakening) of boron layers by charge transfer.

This significant difference may be surprising because Os and Ir have a similar electronegativity of 2.2, the only difference being the occupation of the 5d orbital with 6 and 7 electrons in Os and Ir, respectively. This illustrates the importance of investigating the complex crystal field splitting of the 5d orbitals in the diborides [39,40], and whether the difference in the electronic structure results in different bond deformation paths.

The calculated stress- and energy-strain dependence for the easy slip system [100](001) is shown in Figs. 3(a) and 3(b). The ideal tensile (σ_{min}) and shear (τ_{min}) strengths are summarized in Table I together with those of Os, Ir, Re_3N [14], ReB_2 [30], WB_3 [33], B_6O [34], c-BN [35], and diamond [34,36]. The minimum shear strengths of OsB_2 of 9.2 GPa and IrB_2 of 7.9 GPa are about 4.5 times lower than those of ReB_2, WB_3, and B_6O, and also much lower than those of Os and Ir metals of 22.2 and 18.6 GPa, respectively (Table I). Although OsB_2 and IrB_2 have a similar structure, their bond deformation paths are substantially different, as seen from the VCDD isosurfaces in Figs. 3(c) and 3(d) at shear strain of $\gamma = 0.2899$ (before) and $\gamma = 0.4660$ (after instability) for IrB_2, and $\gamma = 0.2899$ (before) and $\gamma = 0.4660$ (after instability) for OsB_2. For IrB_2, the shear slip occurs between atoms Ir2 and Ir3, which, after the instability, form a single Ir metal layer

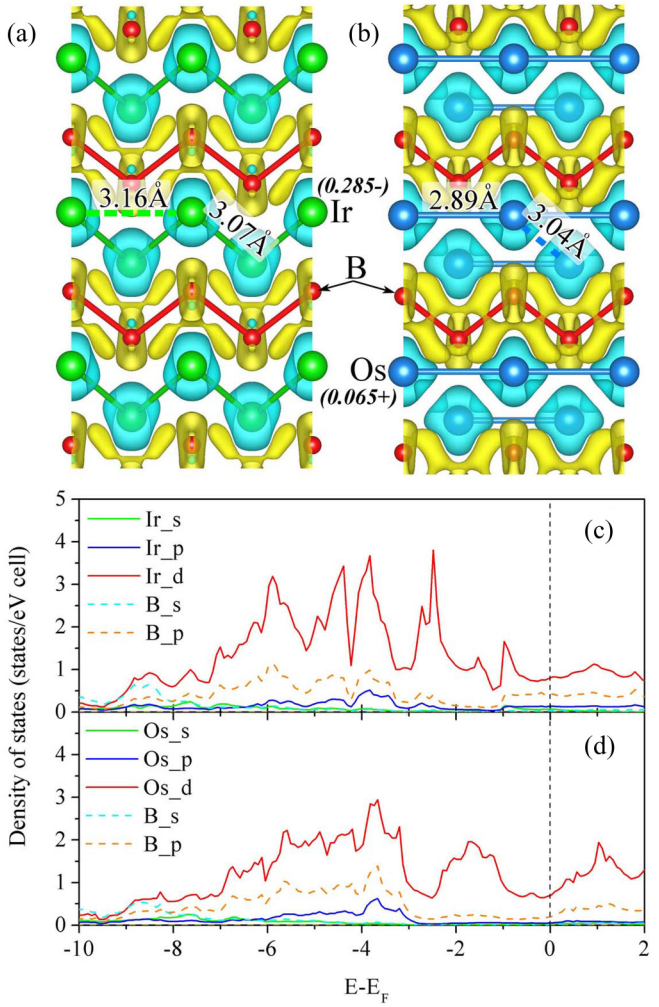

FIG. 2. (Color online) Bond structures at equilibrium for (a) IrB_2 and (b) OsB_2. The isosurface maps of the valence charge density difference (VCDD) correspond to ± 0.01 electrons/bohr^3. Partial electronic density of states of (c) IrB_2 and (d) OsB_2. The numbers close to Ir and Os atoms are the Bader charges.

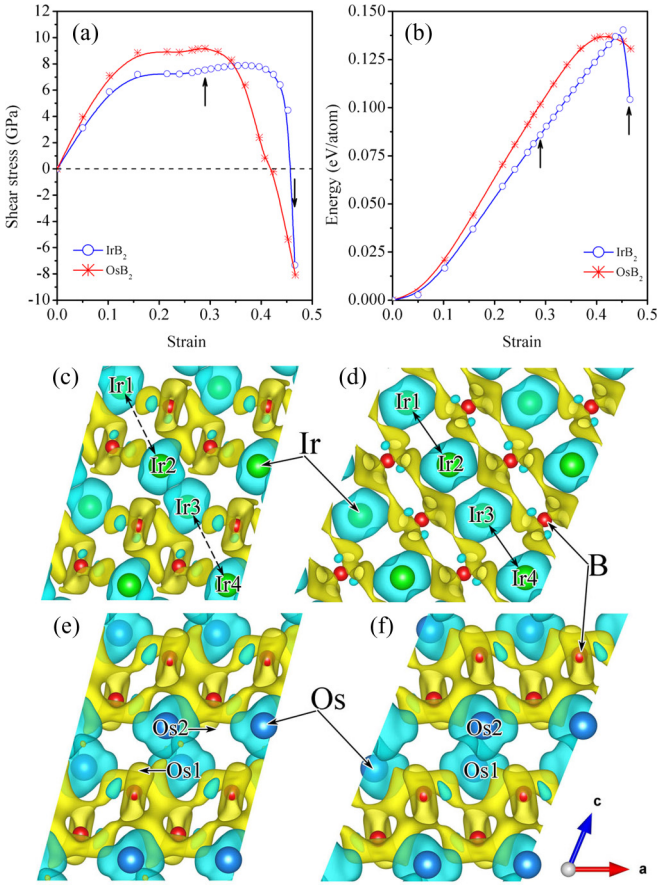

FIG. 3. (Color online) (a) Stress-strain and (b) energy-strain relationships for IrB_2 and OsB_2 along the weakest deformation path [100](001). The isosurfaces of deformed valence charge density difference (VCDD) at shear strain of (c) $\gamma = 0.2899$ (before) and (d) $\gamma = 0.4660$ (after) instability for IrB_2, and (e) $\gamma = 0.2899$ (before) and (f) $\gamma = 0.4660$ (after) instability for OsB_2 in the (001)[100] slip system. The isosurfaces of VCDD correspond to $+/-0.01$ electrons/bohr^3.

Ir1-Ir2-Ir3-Ir4 [Fig. 3(d)]. In OsB_2, however, the shear occurs between Os1 and Os2, which form a double layer.

The decomposed EDOS of 5*d* orbitals of both IrB_2 and OsB_2 before and after shear instability are shown in Figs. 4(a)–4(c) for IrB_2 and in Figs. 4(d)–4(f) for OsB_2 [see the arrows in Figs. 3(a) and 3(b)]. It is seen that before lattice instability, the five 5*d* orbitals do not change their contributions at the Fermi level. The main contribution to the finite value at the Fermi level for IrB_2 comes from the d_{z^2} orbitals, whereas $d_{x^2-y^2}$ orbitals dominate in OsB_2. Therefore the in-plane (xy plane) Ir-Ir bonds are longer than those of the out-of-plane bonds in IrB_2, while in OsB_2 the in-plane Os-Os bond lengths are longer than the out-of-plane lengths. After lattice instability, the d_{yz} and $d_{x^2-y^2}$ orbitals dominate the EDOS in IrB_2 at E_F [Fig. 4(c)], which corresponds to the in-plane splitting of Ir-Ir bonds and the formation of B single layers along the charge-depleting regions [see Fig. 3(d)]. In OsB_2, however, d_{z^2} orbital shows a plateau at E_F, whereas the other four 5*d* orbitals contribute either to the first peaks below E_F or the first peaks above E_F after the instability. These 5*d* electronic instabilities of IrB_2 and OsB_2 resemble those for ReB_2 [10] and WB_3 [33], but the difference is that for the former cases the metallic bonds are responsible for the shear instability, while metal-boron and boron-boron bonds are the carrier of the shear instability in ReB_2 and WB_3.

In order to understand the hardness of the diborides we need to extract the bond strength of Me-B and B-B bonds. We use a "confined" stress-strain experiments by fixing the *Tm-Tm* double layer bonds distance and allowing the Os-B and B-B bonds being the carrier of the shear. The results are shown in Fig. S1 in the Supplemental Material [26] for the weakest [100](001) and [010](001) slip systems. For the [100](001) system we find a high shear strength of 36.6 GPa for OsB_2, comparable to ReB_2 and WB_3 (Table I) and much higher than the shear strength for the unconfined case, where the sliding of the Os-Os planes is dominant. However, a lower value of 15.7 GPa is obtained for IrB_2 where the weaker Ir-B and B-B bonds are limiting the strength, presumably because of the presence of the 7th electron in the upper-laying d_{z^2} and $d_{x^2-y^2}$ orbitals.

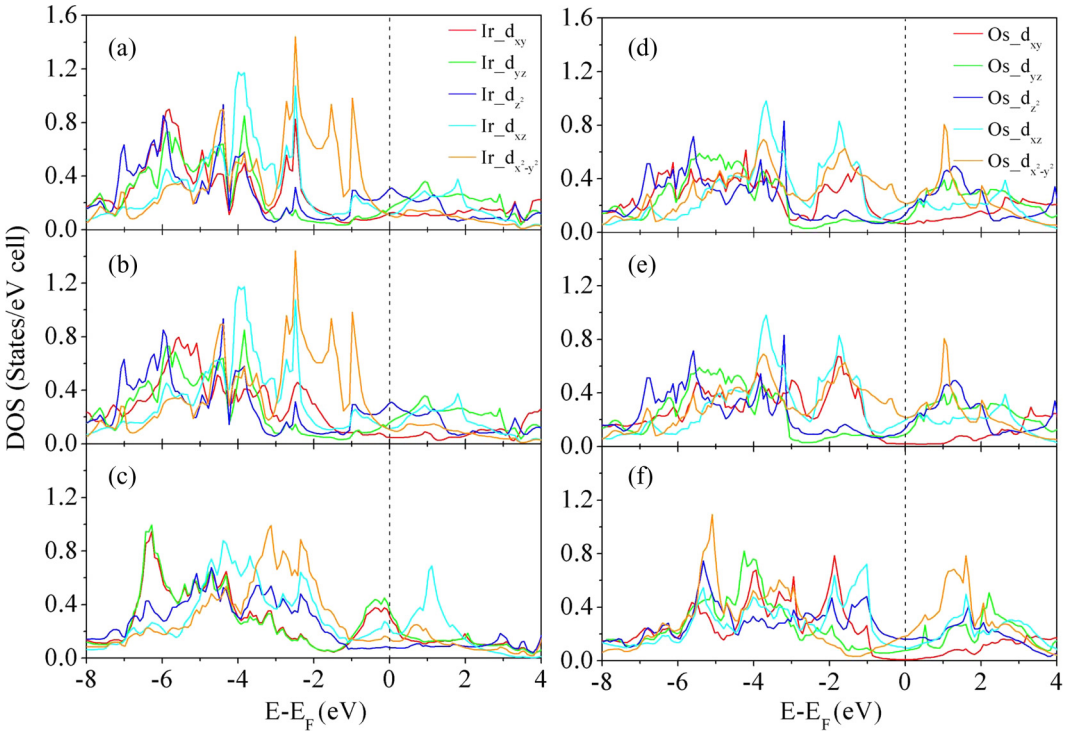

FIG. 4. (Color online) Orbital-decomposed electronic density of states of IrB_2 (a) at equilibrium (b) at strain of 0.2899, (c) at strain of 0.4660, and of OsB_2 (d) at equilibrium (e) at strain of 0.2899, (f) at strain of 0.4660.

In summary, we carried out first-principles calculations to evaluate the thermodynamic, mechanical, and dynamical stabilities of IrB_2 and OsB_2. In spite of its thermodynamic stability, IrB_2 is found to be dynamically unstable. The deformed electronic structure reveals that the low strength is due to the weak metallic bonds, but in a different manner for IrB_2 and OsB_2. The different bond deformation paths are attributed to different electronic instability modes. The high shear strength of Os-B and B-B bonds indicates that they are responsible for the high hardness, in spite of the weak Os-Os bonds. An analysis of the deformed electronic structures reveals that the electronic instability is due to d orbitals of Ir or Os, and p orbitals of B. The orbital-decomposed EDOS show that the d_{z^2} orbitals are mostly responsible for the shear instability of IrB_2, whereas $d_{x^2-y^2}$ orbitals are responsible for the shear instability in OsB_2.

R.F.Z. acknowledges support from the Air Force Office of Scientific Research (Grant No. FA9550-12-1-0456) and NSF (Grant No. DMR-1307840), the Zhuo-Yue Hundred Talents Plan of Beihang University, and the National Thousand Young Talents Program of China. D.L. acknowledges support within the framework of the Nanotechnology—The Basis for International Cooperation project (Reg. No. CZ.1.07/2.3.00/20.0074) and the IT4Innovations Centre of Excellence project (Reg. No. CZ.1.05/1.1.00/02.0070), both supported by Structural Funds of the European Union and the state budget of the Czech Republic. S.V. would like to thank the SHM Company for financial support of his research. K.R. acknowledges support from the Wilkinson Professorship of Interdisciplinary Engineering. We would also like to thank Dr. Maritza Veprek-Heijman for many helpful comments regarding the manuscript.

[1] D. M. Teter and R. J. Hemley, Science **271**, 53 (1996).
[2] S. Veprek, J. Vac. Sci. Technol. A **17**, 2401 (1999); **31**, 050822 (2013).
[3] R. B. Kaner, J. J. Gilman, and S. H. Tolbert, Science **308**, 1268 (2005).
[4] R. W. Cumberland, M. B. Weinberger, J. J. Gilman, S. M. Clark, S. H. Tolbert, and R. B. Kaner, J. Am. Chem. Soc. **127**, 7264 (2005).
[5] H. Y. Chung, M. B. Weinberger, J. B. Levine, A. Kavner, J. M. Yang, S. H. Tolbert, and R. B. Kaner, Science **316**, 436 (2007).
[6] X.-Q. Chen, C. L. Fu, M. Krčmar, and G. S. Painter, Phys. Rev. Lett. **100**, 196403 (2008).
[7] Z. W. Ji, C. H. Hu, D. H. Wang, Y. Zhong, J. Yang, W. Q. Zhang, and H. Y. Zhou, Acta Mater. **60**, 4208 (2012).
[8] R. Mohammadi, A. T. Lech, M. Xie, B. E. Eeaver, M. T. Yeung, S. H. Tolbert, and R. B. Kaner, Proc. Natl. Acad. Sci. USA **108**, 10958 (2011).
[9] J. Yang, H. Sun, and C. F. Chen, J. Am. Chem. Soc. **130**, 7200 (2008).
[10] R. F. Zhang, D. Legut, R. Niewa, A. S. Argon, and S. Veprek, Phys. Rev. B **82**, 104104 (2010).
[11] Q. Gu, G. Krauss, and G. Steurer, Adv. Mater. **20**, 3620 (2008).
[12] J. V. Rau and A. Latini, Chem. Mater. **21**, 1407 (2009).
[13] V. Brazhkin, N. Dubrovinskaia, M. Nicol, N. Novikov, R. Riedel, V. Solozhenko, and Y. Zhao, Nature Mater. **3**, 576 (2004).
[14] R. F. Zhang, Z. J. Lin, H. K. Mao, and Y. S. Zhao, Phys. Rev. B **83**, 060101R (2011).

[15] R. Hill, *The Mathematical Theory of Plasticity* (Clarendon Press, Oxford, 1950).
[16] F. A. McClintock and A. S. Argon, *Mechanical Behavior of Materials* (Addison-Wesley, Reading, MA, 1966).
[17] F. Gao, J. L. He, E. D. Wu, S. M. Liu, D. L. Yu, D. C. Li, S. Y. Zhang, and Y. J. Tian, Phys. Rev. Lett. **91**, 015502 (2003).
[18] A. Simunek and J. Vackar, Phys. Rev. Lett. **96**, 085501 (2006).
[19] M. Wang, Y. W. Li, T. Cui, Y. M. Ma, and G. T. Zou, Appl. Phys. Lett. **93**, 101905 (2008).
[20] S. Veprek, A. S. Argon, and R. F. Zhang, Philos. Mag. **90**, 4101 (2010).
[21] D. Y. Wang, B. Wang, and Y. X. Wang, J. Phys. Chem. C **116**, 21961 (2012).
[22] G. Kresse and J. Furthmüller, Comput. Mater. Sci. **6**, 15 (1996).
[23] FIZ/NIST Inorganic Crystal Structure Database (ICSD) (2009).
[24] S. Curtarolo, G. L. W. Hart, M. B. Nardelli, N. Mingo, S. Sanvito, and O. Levy, Nature Mater. **12**, 191 (2013).
[25] S. Curtarolo, D. Morgan, and G. Ceder, CALPHAD: Comput. Coupling Phase Diagrams Thermochem. **29**, 163 (2005).
[26] See Supplemental Material at http://link.aps.org/supplemental/10.1103/PhysRevB.90.094115 for details of the structure types used for OsB_2 and IrB_2.
[27] K. Parlinski, Z. Q. Li, and Y. Kawazoe, Phys. Rev. Lett. **78**, 4063 (1997).
[28] A. Togo, F. Oba, and I. Tanaka, Phys. Rev. B **78**, 134106 (2008).
[29] G. Grimvall, *Thermophysical Properties of Materials* (Elsevier, Amsterdam, 1999).
[30] R. F. Zhang, S. Veprek, and A. S. Argon, Appl. Phys. Lett. **91**, 201914 (2007).
[31] C. Pantea, I. Stroe, H. Ledbetter, J. B. Betts, Y. Zhao, L. L. Daemen, H. Cynn, and A. Migliori, Phys. Rev. B **80**, 024112 (2009).
[32] D. R. Lide, *CRC Handbook of Chemistry and Physics*, 89th ed. (CRC Press, Boca Raton, FL, 2008), pp. 12–33.
[33] R. F. Zhang, D. Legut, Z. J. Lin, Y. S. Zhao, H. K. Mao, and S. Veprek, Phys. Rev. Lett. **108**, 255502 (2012).
[34] R. F. Zhang, Z. J. Lin, Y. S. Zhao, and S. Veprek, Phys. Rev. B **83**, 092101 (2011).
[35] R. F. Zhang, S. Veprek, and A. S. Argon, Phys. Rev. B **77**, 172103 (2008).
[36] R. F. Zhang, Z. J. Lin, and S. Veprek, Phys. Rev. B **83**, 155452 (2011).
[37] S. F. Pugh, Philos. Mag. **45**, 823 (1954).
[38] R. F. W. Bader, *Atoms in Molecules-A Quantum Theory* (Oxford University Press, Oxford, 1990).
[39] N. N. Greenwood and A. Earnshaw, *Chemistry of the Elements* (Pergamon Press, Oxford, 1984).
[40] T. A. Cotton and G. Wilkinson, *Advanced Inorganic Chemistry*, 3rd ed. (John Wiley & Sons, New York, 1972).